Motorized RhoGAP myosin IXb (Myo9b) controls cell shape and motility

Peter J. Hanley[a,1], Yan Xu[b], Moritz Kronlage[a], Kay Grobe[b,c], Peter Schön[a,d,2], Jian Song[c], Lydia Sorokin[c], Albrecht Schwab[a], and Martin Bähler[b,1]

[a]Institut für Physiologie II, [b]Institut für Molekulare Zellbiologie, and [c]Institut für Physiologische Chemie und Pathobiochemie, Westfälische Wilhems-Universität Münster, 48149 Münster, Germany; and [d]Life Science Team, Veeco Instruments, 68165 Mannheim, Germany

Edited by Peter Devreotes, Johns Hopkins University School of Medicine, Baltimore, MD, and approved May 27, 2010 (received for review October 19, 2009)

Directional motility is a fundamental function of immune cells, which are recruited to sites of pathogen invasion or tissue damage by chemoattractant signals. To move, cells need to generate lamellipodial membrane protrusions at the front and retract the trailing end. These elementary events are initiated by Rho-family GTPases, which cycle between active GTP-bound and inactive GDP-bound states. How the activity of these "molecular switches" is spatially coordinated is only beginning to be understood. Here, we show that myosin IXb (Myo9b), a Rho GTPase-activating protein (RhoGAP) expressed in immune cells, is essential for coordinating the activity of Rho. We generated Myo9b-deficient mice and show that Myo9b$^{-/-}$ macrophages have strikingly defective spreading and polarization. Furthermore, Myo9b$^{-/-}$ macrophages fail to generate lamellipodia in response to a chemoattractant, and migration in a chemotactic gradient is severely impaired. Inhibition of Rho rescues the Myo9b$^{-/-}$ phenotype, but impairs tail retraction. We also found that Myo9b is important in vivo. Chemoattractant-induced monocyte recruitment to the peritoneal cavity is substantially reduced in Myo9b$^{-/-}$ mice. Thus, we identify the "motorized Rho inhibitor" Myo9b as a key molecular component required for spatially coordinated cell shape changes and motility.

cell migration | knockout | Rho-family GTPases | signal transduction

Macrophages and neutrophils are the major functional units of the innate immune system and are rapidly recruited to sites of inflammation or tissue damage by chemoattractant signals (1, 2). To migrate, these cells need to adopt and maintain a polarized morphology, and movement is achieved by coordinately extending thin membrane protrusions (lamellipodia) at the front and retracting the trailing end (1, 3). This basic two-step "amoeboid" type of movement is supported by an intermediate step, the interaction of the protruding membrane with the substrate (1, 3). However, a recent study using pan-integrin knockout leukocytes showed that this intermediate step is not required for the migration of cells in 3D (interstitial) environments (4). Furthermore, using the inhibitor blebbistatin (5), the authors deduced that myosin II-dependent contractile activity was only required to squeeze the rigid nucleus through narrow passages (4). Hence, membrane protrusive activity alone appears to be sufficient to drive migration. Whether one assumes a one-, two-, or three-step model of cell motility, the actin dynamics must be tightly controlled so that the dominant membrane protrusion (leading edge) is confined to the direction of movement. This is achieved by somehow coordinating the activity of the canonical Rho-family GTPases Rac, Cdc42, and Rho, which regulate specific aspects of the protrusion and retraction machinery (3, 6–10).

Rac and Cdc42 act through the Arp2/3 complex to induce the F-actin polymerization driving membrane protrusions at the front, whereas Rho stimulates nonmuscle myosin II-dependent retraction at the rear of migrating cells (6–10). The "on–off" state of these monomeric GTPases is tightly regulated by large families of structurally diverse guanine nucleotide exchange factors (GEFs) and GTPase-activating proteins (GAPs) (11, 12). In addition, guanine nucleotide-dissociation inhibitors sequester and block Rho GTPases (12). GEFs "turn on" Rho GTPases by catalyzing the exchange of GDP for GTP, whereas GAPs "turn off" Rho GTPases by stimulating the hydrolysis of bound GTP. How the activity of Rho GTPases is spatiotemporally regulated in the cell is not well understood, and it is also unclear which GEFs and GAPs are critically involved in regulating the cytoskeletal rearrangements during movement.

Mammalian class IX myosins, consisting of myosin IXa (Myo9a) and myosin IXb (Myo9b), are single-headed molecular motors containing a Rho-specific GAP domain in the tail region. Myo9a (myr 7) is largely expressed in the testis and brain, and mice lacking Myo9a have recently been reported to develop severe hydrocephalus (13). In contrast, Myo9b (myr 5) is predominantly expressed in the immune system (14), and therefore this motorized RhoGAP is a candidate signal molecule for regulating the rapid cell shape changes and motility paramount for host defense. Structurally, Myo9b additionally contains four "IQ" motifs (binding sites for myosin light chains) in its neck region and a C1 (Zn^{2+} binding) domain close to the RhoGAP domain (14–17). Sliding filament assays indicate that Myo9b is a plus-end-directed processive motor (18, 19), but see Inoue et al. (20). The mechanism by which single-headed Myo9b moves appreciable distances along F-actin filaments before it dissociates may involve F-actin tethering by the extended loop 2 (21).

Here, we produced Myo9b-deficient (Myo9b$^{-/-}$) mice, and we revealed that the RhoGAP Myo9b is a key upstream signaling molecule in the control of membrane protrusions and retractions. Myo9b$^{-/-}$ macrophages have a "contracted" morphology characterized by a paucity of lamellipodia and cytoskeletal polarization. Rho signaling is overactive in these cells, and the morphological phenotype can be dramatically rescued by treatment with a Rho inhibitor. Functionally, the velocity of movement of Myo9b$^{-/-}$ macrophages in a chemotactic gradient is very low, and a Rho-specific inhibitor restores motility but prevents tail retraction. Furthermore, we show that chemoattractant-induced recruitment of monocytes to the peritoneum is abrogated in Myo9b$^{-/-}$ mice. It is surprising that a single GAP plays such a decisive role in coordinating membrane protrusions and retractions, although Myo9b has the unique properties of being both a signal molecule (RhoGAP) and an actin-based motor.

Author contributions: P.J.H., Y.X., J.S., L.S., A.S., and M.B. designed research; P.J.H., Y.X., M.K., K.G., P.S., and J.S. performed research; P.J.H., Y.X., M.K., P.S., J.S., and M.B. analyzed data; and P.J.H. and M.B. wrote the paper.

The authors declare no conflict of interest.

This article is a PNAS Direct Submission.

[1]To whom correspondence may be addressed. E-mail: hanley@uni-muenster.de or baehler@uni-muenster.de.

[2]Present address: Materials Science and Technology of Polymers, MESA+ Institute for Nanotechnology, University of Twente, 7500 Enschede, The Netherlands.

This article contains supporting information online at www.pnas.org/lookup/suppl/doi:10.1073/pnas.0911986107/-/DCSupplemental.

Results

Generation of Myo9b-Deficient Mice and Myo9b$^{-/-}$ Macrophage Phenotype. Myo9b$^{-/-}$ mice were generated using the cre-loxP system and homologous recombination in embryonic stem cells (Fig. S1). We constructed a gene-targeting vector by positioning *loxP* sites flanking exon 2 and by placing flippase recognition sites flanking a neomycin-resistance gene. Heterozygous Myo9b$^{+/-}$ mice, obtained by breeding chimeric mice with Flippase transgenic mice and crossing the offspring with Cre-recombinase transgenic mice, were interbred to generate Myo9b$^{-/-}$ mice, which were subsequently backcrossed onto a C57BL/6 background.

Consistent with the previously reported high Myo9b mRNA expression in the immune system (14), we found that Myo9b protein was expressed in WT, but not Myo9b$^{-/-}$, mouse spleen, thymus, and isolated immune cells (Fig. S2*A*). Using lysates from purified resident peritoneal macrophages (F4/80^{+} cells), we could detect the two known splice forms (22) of Myo9b (Fig. 1*A*); myosin IXa (Myo9a) was not detected in either wild-type (WT) or Myo9b-deficient macrophages (Fig. 1*A*). Myo9a is predominantly found in the brain (13, 23, 24) and accordingly we used mouse brain as a positive control in our Western blot analysis (Fig. 1*A*). Confocal fluorescence microscopy indicated that Myo9b is localized to the leading edge of polarized cells (Fig. S2*B*), consistent with recent observations in mouse melanoma (B16/F1) cells (25).

Typically, resident macrophages freshly isolated from the mouse peritoneum have a spherical morphology, but spread and polarize during overnight incubation (Fig. 1*B*). Myo9b$^{-/-}$ macrophages, however, failed to spread and polarize (Fig. 1*B*), such that the projected 2D area was only 130 ± 4 μm^2 (n = 162) in knockout versus 692 ± 25 μm^2 (n = 79) in WT cells. We speculated that decreased Rho-specific GAP activity was responsible for the morphological phenotype in Myo9b-deficient cells. GST-pull down assays revealed that active RhoA (RhoA-GTP) levels were much higher (~6-fold) in Myo9b$^{-/-}$ than WT macrophages, whereas there were no differences in Cdc42 and Rac1 activity (Fig. 1*C*). Consistent with overactive Rho signaling (schematically illustrated in Fig. 1*D*) in Myo9b$^{-/-}$ macrophages, we found that phosphorylated myosin light chain (p-MLC) was increased 2.7 ± 0.4-fold (n = 4) and the inactive phosphorylated form of cofilin (p-cofilin) was increased 2.9 ± 0.3 fold (n = 4) in comparison with WT cells (Fig. 1*E*).

The defective spreading and morphological polarization of Myo9b$^{-/-}$ macrophages was rescued by the TAT-C3 exoenzyme fusion protein (50 μg/mL; TAT confers membrane permeability and the *Clostridium botulinum* toxin C3 inhibits Rho), and to a lesser extent by the downstream Rho kinase (ROCK) inhibitor Y-27632 (10 μM) (Fig. 1 *F* and *G*, Movie S1, and Movie S2). Y-27632 inhibits the two ROCK isoforms p160ROCK (ROCKI) and ROCKII by competitively inhibiting ATP binding (26), but it has also been reported to inhibit PRK-2 (protein kinase C-related protein kinase-2) with similar potency (27). In WT macrophages, TAT-C3 and Y-27632 induced modest spreading (Fig. 1*G*). C3 (and TAT-C3) ADP ribosylates and blocks all three isoforms of Rho (RhoA, RhoB, and RhoC), but mouse peritoneal macrophages express only RhoA and RhoB (28). RhoA is probably the main isoform involved in motility, and both purified native Myo9b and recombinant Myo9b GAP domain have been shown in vitro to "turn off" RhoA (14, 15, 29).

Myo9b Deficiency Impairs Motility and Chemotaxis. To investigate whether gradient sensing and motility are affected by genetic deletion of Myo9b, we established a chemotaxis assay for macrophages using the Ibidi μ-slide chemotaxis chamber. Macrophages were seeded into the narrow channel separating the two 40-μL reservoirs, and the chemoattractant complement component C5a (Mw ~ 9 kDa) was added to one of the reservoirs (final concentration, 10 nM) to establish a spatially well defined chemotactic gradient (Fig. 2*A*). Alternatively, we added Alexa Fluor 488-conjugated dextran (Mw ~ 10 kDa) to one of the reservoirs and measured the gradient in the narrow channel by confocal laser scanning microscopy (Fig. 2*B*). At between 6 and 12 h, a steep gradient could be detected, and we subsequently analyzed macrophage migration in this period. WT macrophages migrated

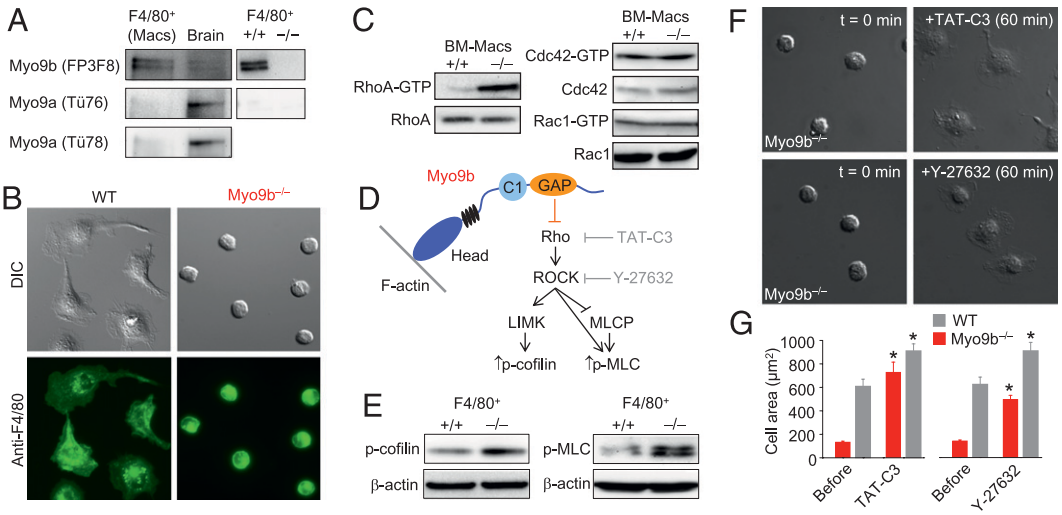

Fig. 1. Myo9b expression in macrophages and rescue of the Myo9b$^{-/-}$ phenotype. (*A*) Myo9b, but not myosin IXa (Myo9a), was detected in resident peritoneal F4/80^{+} cells (F4/80 is a specific marker for mouse macrophages) by Western blot analysis. Neither Myo9b nor Myo9a expression could be detected in Myo9b$^{-/-}$ macrophages. (*B*) Live-cell differential interference contrast (DIC) and fluorescence images (100 × 100 μm) of WT and Myo9b$^{-/-}$ macrophages after overnight incubation. Cells were labeled with Alexa Fluor 488-conjugated anti-F4/80 antibodies. (*C*) Activity of Rho-family GTPases. GST-pull down and Western blot analysis of RhoA, Rac1, and Cdc42 activities in WT versus Myo9b$^{-/-}$ macrophages. (*D*) Schematic diagram showing physiological (Myo9b) and pharmacological (TAT-C3 and Y-27632) inhibition of the Rho signaling pathway. (*E*) Western blot analysis of phosphorylated cofilin (p-cofilin) and myosin light chain (p-MLC) in macrophages. (*F*) Time-lapse DIC images (100 × 100 μm) of Myo9b$^{-/-}$ macrophages after the application of the Rho-specific inhibitor TAT-C3 (50 μg/mL) or ROCK inhibitor Y-27632 (10 μM). (*G*) Mean 2D cell area of Myo9b$^{-/-}$ and WT macrophages before and 60 min after applying TAT-C3 or Y-27632. *P < 0.05 (before versus after treatment, paired t test) and data obtained from three to four independent paired experiments per group.

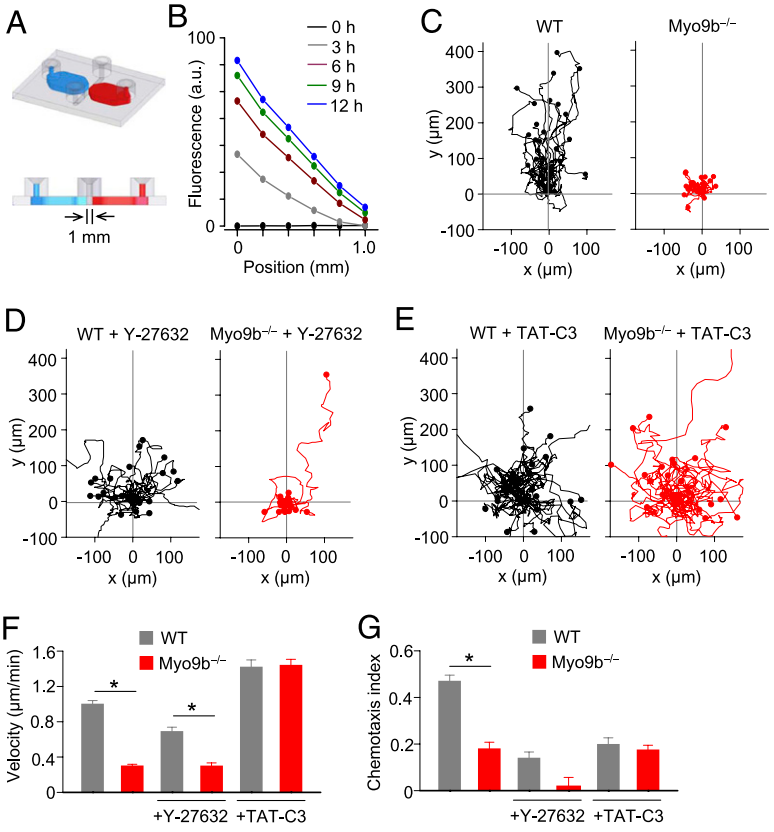

Fig. 2. Impaired motility of Myo9b$^{-/-}$ macrophages. (*A*) Schematic diagram of the μ-slide chemotaxis chamber. Cells were seeded in the narrow channel separating the two reservoirs, one of which contained the chemoattractant C5a (10 nM). (*B*) Kinetics of gradient formation in the narrow chamber, measured by confocal laser scanning microscopy when C5a was replaced by Alexa Fluor 488-labeled dextran. (*C–G*) Chemotaxis assays. (*C*) The migration tracks of 25 WT and 25 Myo9b$^{-/-}$ cells were plotted after normalizing the start point to $x = 0$ and $y = 0$. The y axis represents the direction toward the source of chemoattractant. (*D*) Migration plots of WT and Myo9b$^{-/-}$ cells in the presence of Y-27632. (*E*) Migration plots of WT and Myo9b$^{-/-}$ cells in the presence of TAT-C3. (*F*) Summary plot of mean velocity. (*G*) Summary plot of chemotaxis index. *$P < 0.05$ [Kruskal–Wallis test and post hoc Nemenyi test (*F* and *G*); data obtained from four to five independent experiments per group].

with a mean velocity of 1.0 ± 0.04 μm/min (n = 125) over 6 h, and the chemotactic efficiency, indexed as chemotaxis index, was 0.47 ± 0.03 (Fig. 2*C* and Movie S3). In contrast, Myo9b$^{-/-}$ macrophages migrated with a strikingly reduced velocity and impaired chemotaxis efficiency: mean migration velocity was 0.3 ± 0.02 μm/min (n = 125) and the chemotaxis index was 0.18 ± 0.03 (Fig. 2*C* and Movie S4). There was no significant decline in migration velocity during the analysis period (Fig. S3).

Myo9b$^{-/-}$ macrophage motility was dramatically rescued by TAT-C3 but was little affected by the ROCK inhibitor Y-27632 (Fig. 2 *D–G*, Movie S5, Movie S6, Movie S7, and Movie S8). In terms of velocity and chemotactic efficiency, Myo9b$^{-/-}$ + TAT-C3 and WT + TAT-C3 cells were indistinguishable. However, TAT-C3 induced extremely long branched tails and impaired chemotaxis in both Myo9b$^{-/-}$ and WT cells (Fig. 2*G* and Fig. S4). In addition, Y-27632 induced elongated tails in WT macrophages migrating in a chemotactic gradient (Movie S5). Long tails were also observed in the subpopulation of Myo9b$^{-/-}$ macrophages in which motility was rescued by Y-27632 (Movie S6).

Myo9b Is Required for the Generation of Membrane Protrusions. Myo9b$^{-/-}$ macrophages migrated toward the chemoattractant C5a with a poorly defined tail and a paucity of lamellipodia (Movie S4), indicating that chemotactic cues are not being efficiently translated into membrane protrusions. Using time-lapse differential interference contrast (DIC) imaging, we found that WT macrophages rapidly extended lamellipodia within 90 s of applying C5a (Fig. 3*A* and Movie S9), such that 2D cell area increased from 700 ± 45 to 1039 ± 64 μm^2 [n = 11 (Fig. 3*B*)]. The 2D area of Myo9b$^{-/-}$ macrophages was increased to a lesser extent (from 133 ± 10 to 343 ± 26 μm^2; n = 26) by application of C5a (Fig. 3 *C* and *D* and Movie S10). The most striking difference was that Myo9b$^{-/-}$ cells did not generate the large sheet-like membrane protrusions characteristic of lamellipodia (8). This could not be explained by impaired "chemoattractant-induced" Rac activation because no differences in basal and C5a-induced Rac1-GTP (activated Rac1) levels could be detected between WT and Myo9b$^{-/-}$ macrophages (Fig. S5).

The 3D morphological features of membrane protrusions cannot be quantitatively assessed by DIC imaging. Therefore, we used atomic force microscopy (AFM) to generate high-resolution topographic images of WT versus Myo9b$^{-/-}$ macrophages stimulated with chemoattractant. WT and Myo9b$^{-/-}$ macrophages were fixed ~180 s after C5a challenge and imaged in aqueous solution by AFM in contact mode. Broad lamellipodia, defined as membrane protrusions < 200 nm height (8), dominated the landscape (55 ± 1.5% of the top-view area; n = 5) of C5a-stimulated WT cells (Fig. 3*E*). Membrane waves (ruffles) could be easily distinguished by zooming in on topographic images, which are essentially 3D snapshots of cell dynamics. In contrast to WT cells, only a narrow lamellipodial rim, accounting for 7.9 ± 1.9% of the top-view area (n = 6), could be detected in Myo9b$^{-/-}$ cells stimulated with chemoattractant (Fig. 3*F*). Instead of large lamellipodia, Myo9b$^{-/-}$ macrophages generated transient thick ruffles and flattened in response to chemoattractant (Fig. 3 *C* and *F*).

Ultimately, coordinated actin dynamics allow cells to change shape and move. However, it is difficult to predict the effect of Myo9b (RhoGAP) deficiency on actin polymerization and filament assembly because Rho regulates a number of effectors, including the actin-binding protein cofilin and members of the formin family, such as mDia (7). We therefore imaged and quantified F-actin in fixed and permeabilized macrophages using fluorescently labeled phalloidin (Figs. S6 and S7). Conventional widefield fluorescence images of WT macrophages revealed diffuse F-actin staining in WT macrophages with actin enrichment in peripheral ruffles (Fig. S6*A*). In contrast, Myo9b$^{-/-}$ cells typically displayed a cortical ring of actin (Fig. S6*A*). Super-resolution structured illumination microscopy (SR-SIM) of the same preparations using a prototype Elyra microscope (Zeiss) provided greatly improved structural resolution

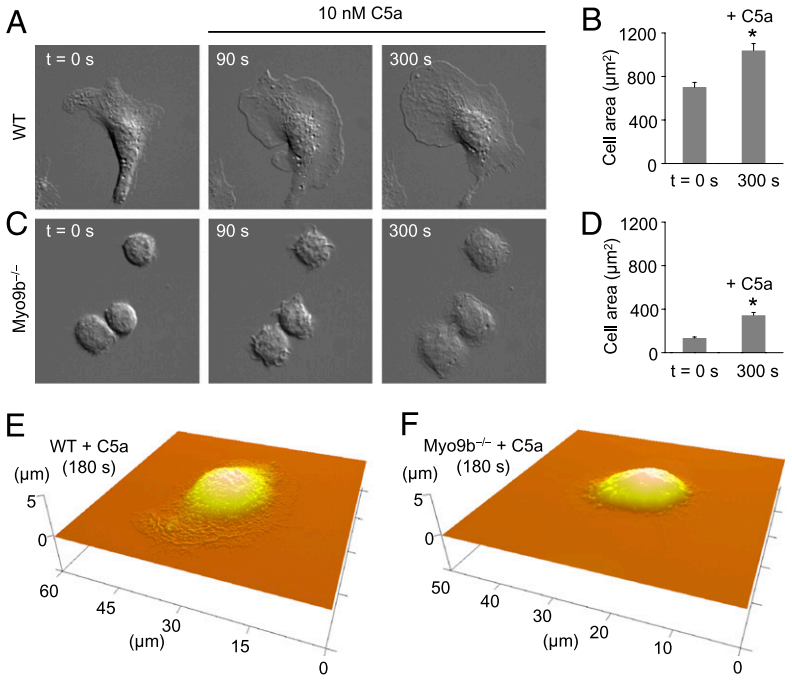

Fig. 3. Lack of membrane protrusive activity in Myo9b$^{-/-}$ macrophages. (*A*) Time-lapse DIC images of WT macrophages following the application of the chemoattractant C5a (Movie S9). (*B*) 2D cell area before and 300 s after application of C5a to WT cells (data from three independent experiments). (*C*) Time-lapse DIC images of Myo9b$^{-/-}$ macrophages following the application of C5a (Movie S10). (*D*) 2D cell area before and 300 s after application of C5a to Myo9b$^{-/-}$ cells (data from four independent experiments). (*E* and *F*) High-resolution 3D surface plots of WT and Myo9b$^{-/-}$ macrophages fixed ~180 s after C5a application. The cells were scanned by AFM in phosphate-buffered solution. *$P < 0.05$ [paired *t* test (*B* and *D*)].

(Fig. S6*B*). SR-SIM images of polarized WT macrophages revealed stress fibers predominantly located at the rear of the cell and actin enrichment at the leading edge (Fig. S6*B*). In contrast, actin-based stress fibers could be identified running circumferentially in Myo9b$^{-/-}$ macrophages (Fig. S6*B*). Notably, WT and Myo9b$^{-/-}$ macrophages treated with recombinant TAT-C3 lacked stress fibers and contained similar amounts of F-actin (Fig. S7). Without TAT-C3 treatment, the total F-actin content of cells (cell area × fluorescence intensity) was higher in WT than in Myo9b$^{-/-}$ macrophages (Fig. S7*C*), although the mean (pixel) fluorescence intensity was higher in knockout cells (Fig. S7*D*). Surprisingly, the cell volumes of WT and Myo9b$^{-/-}$ macrophages, measured by AFM (Fig. S7*E*) or flow cytometry (Fig. S7*F*), were the same, as schematically illustrated in Fig. S7*G*.

Impaired Monocyte Recruitment in Myo9b$^{-/-}$ Mice. Taken together, our in vitro studies show that Myo9b-deficient macrophages have severe defects in morphological polarization, motility, and chemotaxis. In particular, membrane protrusive activity, a major determinant of migration efficiency in tissue (4), is defective in knockout cells. To determine whether Myo9b is important in vivo, we examined mononuclear phagocyte recruitment using an experimental model of C5a-induced peritonitis. Accumulation of Gr-1^{low}F4/80^{high} cells (monocytes and macrophages) in the peritoneal cavity was severely reduced in Myo9b$^{-/-}$ mice in comparison with WT animals (Fig. 4 *A* and *B*): $5.90 \pm 0.89 \times 10^5$ F4/80$^+$ cells accumulated in WT mice ($n = 6$) compared with $1.26 \pm 0.23 \times 10^5$ F4/80$^+$ cells in Myo9b$^{-/-}$ mice ($n = 6$), a 79% reduction (Fig. 4*B*).

Discussion

Since the milestone studies in 1992 (30, 31), Rho-family GTPases have emerged as master switches controlling the cytoskeletal rearrangements underlying fundamental cell functions, including polarization, contraction, and motility (32). However, identifying the molecular components spatially regulating these switches has been a major challenge (33). Here, we generated Myo9b$^{-/-}$ mice and have shown that the RhoGAP Myo9b is essential for the negative regulation of Rho. There is no compensatory expression of Myo9a in Myo9b$^{-/-}$ macrophages, and the total levels of the canonical GTPases RhoA, Cdc42, and Rac1 remain essentially unchanged. Given the large estimate of Rho-family GAPs (~70) expressed in mammals (12, 34, 35), we were surprised that RhoA-GTP levels were markedly elevated in macrophages lacking a single family member. Downstream of Rho, the ROCK-LIMK and ROCK-MLCP signal pathways were overactive in Myo9b-deficient macrophages, and the cells had a striking phenotype. The Rho-specific inhibitor TAT-C3 rescued the aberrant round-shaped morphology of Myo9b$^{-/-}$ macrophages more effectively than the ROCK inhibitor Y-27632, suggesting that a ROCK-independent pathway, such as mDia (36), may contribute to the knockout phenotype.

Migration velocity was severely impaired in Myo9b$^{-/-}$ macrophages, and individual cells moved with a paucity of lamellipodia. Although Y-27632 induced lamellipodia formation, this inhibitor failed to restore motility. In contrast, TAT-C3 greatly increased the velocity of Myo9b$^{-/-}$ macrophages, and the cells had an exaggerated morphological polarity due to the development of extremely long and branched tails, frequently exceeding 100 μm in length. Long tails were also seen in WT cells treated with TAT-C3. Despite impaired tail retraction, TAT-C3 increased the mean velocity of both Myo9b$^{-/-}$ and WT cells to a level ~40% faster than untreated WT cells. One interpretation of these results is that TAT-C3, but not Y-27632, inhibits a ROCK-independent Rho signaling limb that normally acts as a "brake" on motility. Such a brake may prohibit the polarization of cells. Because the exoenzyme C3 has been reported to induce elongated trailing ends, but decrease motility, in human neutrophils (37), future studies are needed to explore the effects of TAT-C3 (and Myo9b deficiency) on mouse neutrophil migration in a chemotactic gradient.

Consistent with our findings, Pixley et al. (38) reported that bone marrow-derived macrophages from BCL6-deficient mice have increased Rho activity associated with impaired cell spreading and motility, assessed using transwell (Boyden chamber) assays. We additionally found that the chemoattractant complement component C5a failed to induce morphological polarization in Myo9b$^{-/-}$ macrophages. Similarly, it has been reported that the chemoattractant fMLP (*N*-formyl-methionyl-leucyl-phenylalanine) fails to induce morphological polarization in neutrophils (differentiated HL-60 cells) transiently expressing constitutively active Rho (10).

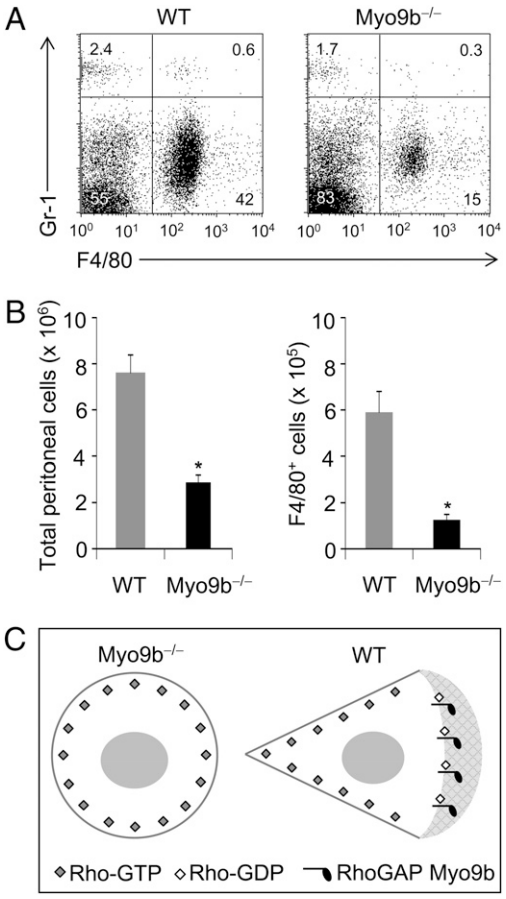

Fig. 4. Impaired Myo9b$^{-/-}$ monocyte/macrophage recruitment in vivo and schematic diagram of Myo9b signaling. (*A*) Flow cytometry of anti-Gr-1 and anti-F4/80 stained cells harvested from the peritoneal cavity 16 h after i.p. injection of C5a. Each dot plot is representative of six independent experiments. Numbers in the quadrants indicate the percentage of cells. (*B*) Mean number (n = 6 mice per group) of total and F4/80$^+$ cells isolated from the peritoneal cavity of WT or Myo9b$^{-/-}$ mice. *, $P < 0.05$ (unpaired t test). (*C*) Proposed model by which the motorized RhoGAP Myo9b controls macrophage polarity and motility. Cells lacking myosin IXb (Myo9b$^{-/-}$) have globally active Rho (Rho-GTP), which decreases actin dynamics and promotes contraction. In WT cells, Myo9b is recruited to the leading edge and catalyzes the hydrolysis of Rho-GTP to its inactive Rho-GDP state.

The authors additionally reported that fMLP fails to induce Rac1 in these cells. In contrast, we found that C5a similarly increased Rac1 activation in WT and Myo9b$^{-/-}$ macrophages, and no differences in the Rac1 activity of resting WT and Myo9b$^{-/-}$ (overactive Rho) could be detected. The extent and mechanism of mutual antagonism between Rac and Rho are controversial, although recent advances in the spatiotemporal imaging of Rho GTPase activities should help resolve these issues (39–41). Surprising in relation to our results, constitutively active Rho has been shown to increase the transendothelial migration of monocytes (NR8383 cells) (42). Although we found that C5a-induced monocyte recruitment to the peritoneum is markedly impaired in Myo9b$^{-/-}$ mice, it would be useful to explore how Myo9b deficiency (and increased Rho activity) affects monocyte migration across different structures, including the endothelium and basement membrane.

In simple models of motility, Rac drives membrane protrusions at the front, whereas Rho acts at the back of the cell to retract the trailing end (1, 3). Consistent with this basic scheme, photoactivation of a Rac1 analog on the edge of cells has recently been shown to induce local membrane protrusions, and repeated light-induced activation enabled control of cell direction (39). Furthermore, inhibition of Rho with TAT-C3 severely impairs tail retraction, underscoring a critical role for Rho in retraction. Hence, coordinated activation of Rac at the front and Rho at the back of migrating cells can explain the elementary events of the protrusion–retraction cycle. Superimposed on this model, a complex spatiotemporal coordination of Rac1, Cdc42, and RhoA activation has been shown to control the contours of the leading edge (40, 41). Missing from these models are molecular mechanisms to switch the Rho-family GTPases "on" and "off." The lack of membrane protrusions in Myo9b-deficient cells, the long tails associated with global Rho inhibition, and the anti-Myo9b labeling at the leading edge (25) suggest that Myo9b plays a pivotal role in shape control and motility, as illustrated in Fig. 4*C*. In basic terms, Myo9b "turns off" Rho at the front, allowing membrane protrusions, and the absence of Myo9b at the back leaves Rho "turned on," thereby promoting tail retraction. PDZRhoGEF may contribute to the fine tuning of Rho activity at the back of migrating cells (43). During motility, the motor protein Myo9b probably moves toward the plus-end of polymerizing actin filaments and catalyzes the hydrolysis of membrane tethered Rho-GTP as it goes.

The rapid recruitment of phagocytic cells to inflammatory "hot spots" is a basic function of the innate immune system. Given the profound effect of Myo9b deficiency on membrane protrusive activity and motility, it would be reasonable to expect that monocyte recruitment is impaired in vivo. Indeed, we found that the accumulation of monocytes and macrophages in the peritoneal cavity of Myo9b$^{-/-}$ mice intraperitoneally injected with the chemoattractant C5a was severely blunted. Hence, Myo9b clearly has an important function in innate immune responses. Another essential function of professional "big eaters" such as macrophages is phagocytosis. Rho-family GTPases are intimately involved in controlling the cytoskeletal dynamics during phagocytosis (44), and we would predict that Myo9b is also important for the local coordination of membrane extensions and particle internalization.

In summary, the small GTPase Rho is one of the "big bosses" controlling cell shape and motility. This study identifies the "motorized signal molecule" Myo9b as a key negative regulator of Rho. Myo9b-deficient cells have overactive Rho signaling pathways, an aberrant rounded phenotype, and severely impaired motility. Inhibition of Rho with recombinant TAT-C3 restores membrane protrusive activity and motility, but prevents tail retraction. Hence, the RhoGAP Myo9b is required for spatially coordinated membrane protrusions and retractions, the elementary events underlying shape changes and directional motility. Future studies are needed to delineate the signal-transduction mechanisms linking extracellular signals to the motor and GAP activities of Myo9b.

Materials and Methods

Myosin IXb (Myo9b) Knockout Mice. The generation of Myo9b$^{-/-}$ mice is described in *SI Materials and Methods*.

Isolation of Resident Peritoneal Macrophages. Mice were killed by an overdose of the volatile anesthetic isoflurane, and resident cells were obtained by lavage of the peritoneal cavity with ice-cold HBSS via a plastic catheter. More details are provided in *SI Materials and Methods*.

Purification of Macrophages. Macrophages were labeled with rat Alexa Fluor 488-conjugated anti-mouse F4/80 antibodies, and F4/80$^+$ cells were isolated using a FACSCalibur flow cytometer (BD Biosciences).

Western Blot Analysis. Proteins were extracted from tissues or cells using lysis buffer and separated by SDS polyacrylamide gel electrophoresis before transfer onto poly(vinylidene difluoride) membranes. After blocking, membranes were probed with primary antibody overnight. Horseradish peroxidase-conjugated secondary antibodies and SuperSignal West Pico chemiluminescence substrate were used for detection. More details are provided in *SI Materials and Methods*.

Live-Cell Imaging. Fibronectin-coated μ-slide I or μ-slide chemotaxis chambers (Ibidi) were placed on the stage of an inverted AxioObserver microscope (Zeiss) fitted with a temperature-controlled incubator. Macrophages were imaged via a 63×/1.4 oil-immersion objective, and time-lapse images were made using Zeiss AxioVision software.

Confocal Microscopy. Fixed and permeabilized macrophages were labeled with anti-Myo9b antibodies, and confocal fluorescence images were obtained via a 63×/1.4 oil-immersion objective using an LSM 510 microscope (Zeiss).

Superresolution Structured Illumination Microscopy. The distribution and quantity of fluorescently labeled F-actin in fixed and permeabilized macrophages was investigated by conventional widefield fluorescence and superresolution structured illumination microscopy (SR-SIM) using a prototype high-resolution Elyra microscope (Zeiss). More details are provided in *SI Materials and Methods*.

Bone Marrow-Derived Macrophages. To obtain high cell numbers for the analysis of Rho-family GTPase levels and activity, macrophages were derived from bone marrow cells. Details of the isolation and the culture of bone marrow-derived cells is provided in *SI Materials and Methods*.

Analysis of Rho-Family GTPases. The determination of total and active levels of RhoA, Cdc42, and Rac1 are provided in *SI Materials and Methods*.

Chemotaxis Assays. Macrophages were seeded into the narrow chamber of an Ibidi μ-slide chemotaxis chamber. Chemoattractant (complement component C5a) was added to one of the two 40-μL reservoirs and time-lapse images of the cells were made over 14 h. Cell migration tracks between 6 and 12 h were analyzed using ImageJ (National Institutes of Health) and the Chemotaxis Tool plug-in from Ibidi. More details are provided in *SI Materials and Methods*.

Atomic Force Microscopy. Topographical scans of fixed macrophages were made in phosphate buffer solution using BioScope Catalyst and BioScope II atomic force microscopes (Veeco Instruments, Inc.) coupled to a Leica DMI6000B inverted microscope (Leica Microsystems). More details are provided in *SI Materials and Methods*.

In Vivo Monocyte Recruitment Assay. Complement component C5a was injected into the peritoneal cavity of WT and Myo9b$^{-/-}$ mice. After 16 h, cells were obtained by peritoneal lavage, labeled with fluorescent anti-Gr-1 and anti-F4/80 antibodies, and analyzed by flow cytometry.

ACKNOWLEDGMENTS. We thank A. Fleige for generating 3D images of the chemotaxis chamber and C. Klämbt and S. Bogdan for use and instructions of the Elyra (SIM) microscope. We also thank K. Uhlenbrock for help in constructing the targeting vector. This work was supported in part by Deutsche Forschungsgemeinschaft Grants SFB 629/A2 (to M.B.) and SCHW 407/9-3 (to A.S.) and Innovative Medizinische Forschung Grant HA110710 (to P.J.H.) from Westfälische Wilhems-Universität Münster.

1. Friedl P, Weigelin B (2008) Interstitial leukocyte migration and immune function. *Nat Immunol* 9:960–969.
2. Heit B, et al. (2008) PTEN functions to 'prioritize' chemotactic cues and prevent 'distraction' in migrating neutrophils. *Nat Immunol* 9:743–752.
3. Ridley AJ, et al. (2003) Cell migration: Integrating signals from front to back. *Science* 302:1704–1709.
4. Lämmermann T, et al. (2008) Rapid leukocyte migration by integrin-independent flowing and squeezing. *Nature* 453:51–55.
5. Allingham JS, Smith R, Rayment I (2005) The structural basis of blebbistatin inhibition and specificity for myosin II. *Nat Struct Mol Biol* 12:378–379.
6. Riento K, Ridley AJ (2003) Rocks: Multifunctional kinases in cell behaviour. *Nat Rev Mol Cell Biol* 4:446–456.
7. Jaffe AB, Hall A (2005) Rho GTPases: Biochemistry and biology. *Annu Rev Cell Dev Biol* 21:247–269.
8. Chhabra ES, Higgs HN (2007) The many faces of actin: Matching assembly factors with cellular structures. *Nat Cell Biol* 9:1110–1121.
9. Heasman SJ, Ridley AJ (2008) Mammalian Rho GTPases: New insights into their functions from in vivo studies. *Nat Rev Mol Cell Biol* 9:690–701.
10. Xu J, et al. (2003) Divergent signals and cytoskeletal assemblies regulate self-organizing polarity in neutrophils. *Cell* 114:201–214.
11. Rossman KL, Der CJ, Sondek J (2005) GEF means go: Turning on RHO GTPases with guanine nucleotide-exchange factors. *Nat Rev Mol Cell Biol* 6:167–180.
12. Tcherkezian J, Lamarche-Vane N (2007) Current knowledge of the large RhoGAP family of proteins. *Biol Cell* 99:67–86.
13. Abouhamed M, et al. (2009) Myosin IXa regulates epithelial differentiation and its deficiency results in hydrocephalus. *Mol Biol Cell* 20:5074–5085.
14. Wirth JA, Jensen KA, Post PL, Bement WM, Mooseker MS (1996) Human myosin-IXb, an unconventional myosin with a chimerin-like rho/rac GTPase-activating protein domain in its tail. *J Cell Sci* 109:653–661.
15. Reinhard J, et al. (1995) A novel type of myosin implicated in signalling by rho family GTPases. *EMBO J* 14:697–704.
16. Post PL, Bokoch GM, Mooseker MS (1998) Human myosin-IXb is a mechanochemically active motor and a GAP for rho. *J Cell Sci* 111:941–950.
17. Saeki N, Tokuo H, Ikebe M (2005) BIG1 is a binding partner of myosin IXb and regulates its Rho-GTPase activating protein activity. *J Biol Chem* 280:10128–10134.
18. Post PL, et al. (2002) Myosin-IXb is a single-headed and processive motor. *J Biol Chem* 277:11679–11683.
19. O'Connell CB, Mooseker MS (2003) Native Myosin-IXb is a plus-, not a minus-end-directed motor. *Nat Cell Biol* 5:171–172.
20. Inoue A, Saito J, Ikebe R, Ikebe M (2002) Myosin IXb is a single-headed minus-end-directed processive motor. *Nat Cell Biol* 4:302–306.
21. Struchholz S, et al. (2009) Functional role of the extended loop 2 in the myosin 9b head for binding F-actin. *J Biol Chem* 284:3663–3671.
22. Grewal PK, et al. (1999) Cloning of the murine unconventional myosin gene Myo9b and identification of alternative splicing. *Gene* 240:389–398.
23. Chieregatti E, Gärtner A, Stöffler H-E, Bähler M (1998) Myr 7 is a novel myosin IX-RhoGAP expressed in rat brain. *J Cell Sci* 111:3597–3608.
24. Gorman SW, et al. (1999) The cloning and developmental expression of unconventional myosin IXA (MYO9A) a gene in the Bardet-Biedl syndrome (BBS4) region at chromosome 15q22-q23. *Genomics* 59:150–160.
25. van den Boom F, Düssmann H, Uhlenbrock K, Abouhamed M, Bähler M (2007) The Myosin IXb motor activity targets the myosin IXb RhoGAP domain as cargo to sites of actin polymerization. *Mol Biol Cell* 18:1507–1518.
26. Ishizaki T, et al. (2000) Pharmacological properties of Y-27632, a specific inhibitor of rho-associated kinases. *Mol Pharmacol* 57:976–983.
27. Davies SP, Reddy H, Caivano M, Cohen P (2000) Specificity and mechanism of action of some commonly used protein kinase inhibitors. *Biochem J* 351:95–105.
28. Wheeler AP, Ridley AJ (2007) RhoB affects macrophage adhesion, integrin expression and migration. *Exp Cell Res* 313:3505–3516.
29. Müller RT, Honnert U, Reinhard J, Bähler M (1997) The rat myosin myr 5 is a GTPase-activating protein for Rho in vivo: Essential role of arginine 1695. *Mol Biol Cell* 8: 2039–2053.
30. Ridley AJ, Hall A (1992) The small GTP-binding protein rho regulates the assembly of focal adhesions and actin stress fibers in response to growth factors. *Cell* 70:389–399.
31. Ridley AJ, Paterson HF, Johnston CL, Diekmann D, Hall A (1992) The small GTP-binding protein rac regulates growth factor-induced membrane ruffling. *Cell* 70:401–410.
32. Etienne-Manneville S, Hall A (2002) Rho GTPases in cell biology. *Nature* 420:629–635.
33. Stephens L, Milne L, Hawkins P (2008) Moving towards a better understanding of chemotaxis. *Curr Biol* 18:R485–R494.
34. Bernards A (2003) GAPs galore! A survey of putative Ras superfamily GTPase activating proteins in man and Drosophila. *Biochim Biophys Acta* 1603:47–82.
35. Jiang S-Y, Ramachandran S (2006) Comparative and evolutionary analysis of genes encoding small GTPases and their activating proteins in eukaryotic genomes. *Physiol Genomics* 24:235–251.
36. Lammers M, Meyer S, Kühlmann D, Wittinghofer A (2008) Specificity of interactions between mDia isoforms and Rho proteins. *J Biol Chem* 283:35236–35246.
37. Yoshinaga-Ohara N, Takahashi A, Uchiyama T, Sasada M (2002) Spatiotemporal regulation of moesin phosphorylation and rear release by Rho and serine/threonine phosphatase during neutrophil migration. *Exp Cell Res* 278:112–122.
38. Pixley FJ, et al. (2005) BCL6 suppresses RhoA activity to alter macrophage morphology and motility. *J Cell Sci* 118:1873–1883.
39. Wu YI, et al. (2009) A genetically encoded photoactivatable Rac controls the motility of living cells. *Nature* 461:104–108.
40. Pertz O, Hodgson L, Klemke RL, Hahn KM (2006) Spatiotemporal dynamics of RhoA activity in migrating cells. *Nature* 440:1069–1072.
41. Machacek M, et al. (2009) Coordination of Rho GTPase activities during cell protrusion. *Nature* 461:99–103.
42. Honing H, et al. (2004) RhoA activation promotes transendothelial migration of monocytes via ROCK. *J Leukoc Biol* 75:523–528.
43. Wong K, Van Keymeulen A, Bourne HR (2007) PDZRhoGEF and myosin II localize RhoA activity to the back of polarizing neutrophil-like cells. *J Cell Biol* 179:1141–1148.
44. Chimini G, Chavrier P (2000) Function of Rho family proteins in actin dynamics during phagocytosis and engulfment. *Nat Cell Biol* 2:E191–E196.